RSC Advances

This article can be cited before page numbers have been issued, to do this please use: S. Wang, F. teng and Y. Zhao, *RSC Adv.*, 2015, DOI: 10.1039/C5RA14931B.

ROYAL SOCIETY OF CHEMISTRY

www.rsc.org/advances

View Article Online
DOI: 10.1039/C5RA14931B

Effects of molecule structure and charging property on adsorption and photocatalytic degradation of dye mixture wastewater

Shurong Wang, Fei Teng*, Yunxuan Zhao

Jiangsu Engineering and Technology Research Center of Environmental Cleaning Materials (ECM), Jiangsu Key Laboratory of Atmospheric Environment Monitoring and Pollution Control (AEMPC), Jiangsu Joint Laboratory of Atmospheric Pollution Control (APC), Collaborative Innovation Center of Atmospheric Environment and Equipment Technology (AEET), School of Environmental Science and Engineering, Nanjing University of Information Science & Technology, 219 Ningliu Road, Nanjing 210044, China.

Abstract

The $[Bi_6O_6(OH)_3](NO_3)_3 \cdot 1.5H_2O$ plates are prepared by a facile hydrothermal method. The effects of pH value, hydrothermal temperature, time, the concentration of Bi(III) ion and additive on the samples are investigated. The as-synthesized samples are characterized by X-ray diffraction (XRD), scanning electron microscopy (SEM), high-resolution transmission electron microscopy (TEM), Brunauer-Emmett-Teller (BET) and UV-vis diffuse reflectance spectrum (UV-DRS). It is found that under ultraviolet light irradiation ($\leq$ 420 nm), the sample prepared at pH=0.72 shows a higher photocatalytic activity than those at higher pH values, which has been mainly ascribed to the promoted oxygen adsorption by the low pH value. Moreover, we mainly investigate the effects of molecule structure and charge on adsorption and photocatalytic degradation of dye mixtures (methyl orange (MO)/methylene blue (MB)

* Corresponding author. Email: 001880@nuist.edu.cn (F. Teng); Phone/Fax: +86-25-58731090

View Article Online
DOI: 10.1039/C5RA14931B

and MO/rhodamine B (RhB)). The results show that in the MB/MO mixture, the adsorption and degradation of both MO and MB are promoted greatly via an electrostatic force; while in the RhB/MO mixture, the degradation of RhB are greatly reduced by MO, due to a competitive adsorption. The finding benefits us to understand the degradation process for practical wastewater containing more than one pollutant.

Keywords: Electrostatic force; Competitive adsorption; Degradation; Dye mixture wastewater; $Bi_6O_6(OH)_3](NO_3)_3 \cdot 1.5H_2O$

Main finding

In a dye mixture, their degradation efficiencies of are much different due to their different interactions, which favors to understand the degradation process for practical wastewater.

View Article Online
DOI: 10.1039/C5RA14931B

1. Introduction

Today, water pollution becomes more serious with the developments of chemical industries. Since the discovery of photocatalysis, [1] a large number of photocatalysts have been investigated. However, it remains a big challenge to develop an efficient photocatalyst for the practical application. Among various photocatalysts, bismuth-containing compounds as efficient photocatalysts have been researched intensively. [2-9] Besides, bismuth compounds are easier to be recovered from aqueous system due to its higher molecular weights than TiO_2. To the best of our knowledge, however, only fewer studies [10-13] have reported the plate-like $[Bi_6O_6(OH)_3](NO_3)_3 \cdot 1.5H_2O$ photocatalyst. In the pioneering works, Christensen *et al.* [10] obtained the composition of $[Bi_6O_6(OH)_3](NO_3)_3 \cdot 1.5H_2O$ using thermogravimetric analysis. Xie *et al.* [11] synthesized $[Bi_6O_6(OH)_3](NO_3)_3 \cdot 1.5H_2O$ by a microwave-assisted hydrothermal method. Afterward, Xie *et al.* [12] synthesized the $[Bi_6O_6(OH)_3](NO_3)_3 \cdot 1.5H_2O$ photocatalysts via a hydrothermal method, and investigated the degradation activity of malachite green (MG). Recently, Yang *et al.* [13] investigated the photocatalytic activity of $[Bi_6O_6(OH)_3](NO_3)_3 \cdot 1.5H_2O$ for the degradation of phenol. In these studies above, however, the influences of preparation conditions on $[Bi_6O_6(OH)_3](NO_3)_3 \cdot 1.5H_2O$ have not been investigated intensively. It is well known that preparations conditions have great influences on the performances of materials. It is desirable to investigate in detail the influences of various preparation parameters so as to understand the formation of $[Bi_6O_6(OH)_3](NO_3)_3 \cdot 1.5H_2O$.

Moreover, practical wastewaters generally contain more than one pollutant. As a result, the photocatalytic degradation process of practical wastewater becomes

View Article Online
DOI: 10.1039/C5RA14931B

complicate, even invalid. It is important to clearly understand the mutual interaction among different pollutants components. Nevertheless, this work has been scarcely studied. In this work, we systematically investigated the influences of various preparation parameters on the formation of $[Bi_6O_6(OH)_3](NO_3)_3 \cdot 1.5H_2O$, so as to determine what parameter plays the crucial role in forming $[Bi_6O_6(OH)_3](NO_3)_3 \cdot 1.5H_2O$. Moreover, we have mainly researched the mutual interactions of different dyes in the methyl orange (MO)/methylene blue (MB) and MO/rhodamine B (RhB) mixtures. The study could be useful to promote the development of photocatalysis in practices.

2. Experimental

2.1 Sample preparation

All reagents were of analytical grade, purchased from Beijing Chemical Reagents Industrial Company in China, and were used without further purification.

Typically, 1 mmol of $Bi(NO_3)_3 \cdot 5H_2O$ was dissolved in 20 mL of distilled water, and then 3 mL 1M diluted HNO_3 solution was added into the above solution under magnetic stirring, followed by adding distilled water to form 40 mL of solution. After being magnetically stirred for 30 min, the resulting white suspension was transferred into a Teflon-sealed autoclave and maintained at 180 °C for 24 h. After being cooled to room temperature naturally, the product was separated by centrifugation, washed with distilled water and ethanol for several times, and dried at 60°C for 5 h. The experimental parameters, including pH value, hydrothermal temperature, time, the concentration of Bi(III) ions and ethylene glycol/water ratio, were varied to understand the formation of $[Bi_6O_6(OH)_3](NO_3)_3 \cdot 1.5H_2O$, which was listed in Table

View Article Online
DOI: 10.1039/C5RA14931B

1-3.

2.2 Characterization

The crystal structures of the samples were determined by X-ray powder polycrystalline diffractometer (Rigaku D/max-2550VB), using graphite monochromatized Cu K_α radiation (λ= 0.154 nm), operating at 40 kV and 50mA. The XRD patterns were obtained in the range of 20-80° (2θ) at a scanning rate of 5 ° min^{-1}. The samples were characterized on a scanning electron microscope (SEM, Hitachi SU-1510) with an acceleration voltage of 15 keV. The samples were coated with 5-nm-thick gold layer before observations. The fine surface structures of the samples were determined by high-resolution transmission electron microscopy (HRTEM, JEOL JEM-2100F) equipped with an electron diffraction (ED) attachment with an acceleration voltage of 200 kV. UV-vis diffused reflectance spectra of the samples were obtained using a UV-vis spectrophotometer (UV-2550, Shimadzu, Japan). $BaSO_4$ was used as a reflectance standard in a UV-vis diffuse reflectance experiment. Nitrogen sorption isotherms were performed at 77 K and < 10^{-4} bar on a Micromeritics ASAP2010 gas adsorption analyzer. Each sample was degassed at 150 ºC for 5 h before measurements. Surface area was calculated by the Brunauer-Emmett-Teller (BET) method.

2.3 Photocatalytic activity evaluation

The photocatalytic activities of the samples were evaluated by degradation of MO, MB, RhB, MO/RhB and MB/MO aqueous solutions under ultraviolet light irradiation ($\lambda \leq 420$nm), using a 500 W Xe arc lamp (CEL-HXF 300) equipped with an ultraviolet cutoff filter as a light source. The reaction system was placed in a

View Article Online
DOI: 10.1039/C5RA14931B

sealed black box with the top opened, and a distance of 15 cm was maintained from the solution surface to light source. 100 mg of powders was dispersed in 200 mL of MO(12.5 mg/L), MB(4.5 mg/L), RhB(7.5 mg/L), MO(12.5 mg/L)/RhB(7.5 mg/L) and MO(12.5 mg/L)/MB(4.5 mg/L) aqueous solutions in a Pyrex beaker at room temperature, respectively. Before lamp was turned on, the suspension was continuously stirred for 30 min in the dark to ensure the establishment of an adsorption–desorption equilibrium between the powders and dye molecules. During degradation, 3 mL of solution was collected at intervals of irradiation by pipette, and subsequently centrifuged to remove the catalysts. UV-vis spectra were recorded on a Spectrumlab 722sp spectrophotometer to determine the concentration of dye. The photocatalytic reaction was normalized by an apparent first-order kinetic equation as follows:

$$\ln(C_0/C) = k_a \times t, \text{ or } C = C_0 \times \exp(-k_a \times t) \quad (1)$$

Where C_0 is the initial concentration of dye solution, and C is the concentration of dye molecule at different irradiation time, k_a represents apparent first-order rate constant.

3. Results and discussion

3.1 Effect of pH value on the samples

Table 1 shows the effect of pH value on the samples. The crystal phases of the products are determined by X-ray powder diffraction (XRD) (Fig. 1a). At pH≤5.38, all the diffraction peaks of the samples can be well indexed to tetragonal $[Bi_6O_6(OH)_3](NO_3)_3 \cdot 1.5H_2O$ (a=b=3.8175Å, c=17.149Å, JCPDS: 53-1038). At pH=0.72 and 1.15, the intensities of the diffraction peaks of the samples do not change significantly. At pH=3.51, the intensities of the diffraction peaks of the sample

View Article Online
DOI: 10.1039/C5RA14931B

increase obviously. Generally, a high pH value favors for the hydrolysis of Bi(III). Nevertheless, at too high pH values (7, 9.05), the Bi_2O_3 and NH_4NO_3 have formed. Herein, the hydrolysis of Bi(III) can be described as Equation (2) as follows:

$$Bi(NO_3)_3 \cdot + H_2O \rightarrow Bi_6O_6(OH)_3](NO_3)_3 \cdot 1.5H_2O + H^+ \quad (2)$$

herein, the pH value of the precursor solution was adjusted by adding HNO_3 or $NH_3 \cdot H_2O$. The pH value would affect the crystal nucleation and growth. [14] When HNO_3 was added, the hydrolysis of Bi(III) was restrained. As a result, the large particles, consisting of plates subunits, formed (Fig. 1b). Henry *et al.* [15] has reported that the OH^- and NO_3^- would bond to Bi(III) downward (Bi-OH bonds) and upward (Bi-ONO_2 bonds), respectively; and the inserted OH^- and NO_3^- between $[Bi_2O_2]^{2+}$ layers are connected through the hydrogen bond. Nevertheless, *Li et al.* hold that [16] both OH^- and NO_3^- layers stack together along the *c*-axis via Van der Waals force (nonbonding interactions). Herein we hold that the formation of plate-like subunits could result from the intrinsic anisotropic layered structure of $[Bi_6O_6(OH)_3](NO_3)_3 \cdot 1.5H_2O$. At low pH values, the number of nuclei is fewer, and then the nuclei grow slowly to form $[Bi_6O_6(OH)_3](NO_3)_3 \cdot 1.5H_2O$ plates (Fig. 1(b,c)). [17] At the moderate pH values (3.51, 5.38), $[Bi_6O_6(OH)_3](NO_3)_3 \cdot 1.5H_2O$ plates agglomerate or assemble to form thick biscuits (Fig. 1d). At high pH values (7.36), the thin plates form (Fig. 1e,f), but the impurities phase also form. The high pH value can not only promote crystal nucleation and growth, but also favor for the dehydration of Bi-OH to form Bi_2O_3. It is obvious that the pH value plays a crucial role in the formation of $[Bi_6O_6(OH)_3](NO_3)_3 \cdot 1.5H_2O$.

Typically, the BS1 sample prepared at pH=0.72 was further characterized by high-resolution electron emission microscopy (HRTEM) and selected area electron diffraction (SAED) (Fig. 2). As shown in Fig. 2c, the lattice spacings of 0.317nm,

View Article Online
DOI: 10.1039/C5RA14931B

0.286nm and 0.271 nm are well consistent to the literature data of d_{103}= 3.173 Å, d_{006}= 2.855 Å and d_{110}=2.697 Å of $[Bi_6O_6(OH)_3](NO_3)_3 \cdot 1.5H_2O$, respectively. Furthermore, the diffraction rings result from the (1010) and (006) Bragg reflections (Fig. 2d), revealing the polycrystalline nature of $[Bi_6O_6(OH)_3](NO_3)_3 \cdot 1.5H_2O$.

3.2 Effects of temperature, time, Bi(III) concentration and V_{EG}/V_W on the samples

In order to understand the evolution process of $[Bi_6O_6(OH)_3](NO_3)_3 \cdot 1.5H_2O$, the reaction temperature-, time-, Bi(III) concentration-dependent experiments were carried out (Table 2).

Fig. 3a shows the XRD patterns of the samples prepared at different temperatures. All the as-prepared samples are phase-pure $[Bi_6O_6(OH)_3](NO_3)_3 \cdot 1.5H_2O$ forms (JCPDS: 53-1038) (Fig. 3a), and the large aggregates of plates form (Fig. 3b,c). It is obvious that with the increase of temperature, the peaks intensities increase. A high crystallinity indicates less bulk defects. [18] Usually, the bulk defects of photocatalyst are considered to be the recombination centers for photogenerated holes and electrons, resulting in a low photocatalytic activity. [18] Thus, the sample obtained at high temperatures could be beneficial to improve photocatalytic activity. Fig. 3d shows the XRD patterns of the samples at different reaction times (12-30 h). All the samples are well indexed to the phase-pure $[Bi_6O_6(OH)_3](NO_3)_3 \cdot 1.5H_2O$ (JCPDS: 53-1038) (Fig. 3d). At 12 and 18h, the peaks intensities of the samples do not vary obviously. At 24 and 30 h, the peaks intensities of the samples increase, indicating an increased crystallinity. No obvious difference can be observed from their SEM images (Fig. 3e,f). Fig. 3(g-i) present the XRD patterns and SEM images of the samples at different Bi(III) concentrations. All the samples can also be well indexed to phase-pure

View Article Online
DOI: 10.1039/C5RA14931B

$[Bi_6O_6(OH)_3](NO_3)_3 \cdot 1.5H_2O$, but the product yield increases with increasing Bi(III) concentration. It is obvious that the temperature, time and Bi(III) concentration have little influence on the phase purity and morphology of the sample.

Table 3 and Fig. 4a-f present the effect of volumetric ratio of ethylene glycol/water (V_{EG}/V_W) on the samples. In pure ethylene glycol, only Bi metal form, in which Bi(III) has been reduced by ethylene glycol. [19,20] When V_{EG}/V_W decreases from 3/1 to 1/1, the $Bi_2O_2CO_3$, Bi_2O_3 and an unknown impurities phases form. When V_{EG}/V_W is smaller than 1, the diffraction peaks of metal bismuth disappeared. The phase-pure $[Bi_6O_6(OH)_3](NO_3)_3 \cdot 1.5H_2O$ can be harvested only in pure water. Fig. 4(b,c) shows that in the presence of glycol, the formed microspheres are assembled by thin plates. With increasing V_{EG}/V_W, the sample is tendency to form microsphere. At V_{EG}/V_W=1, most of microspheres have cracked and a few of hollow microspheres have formed (Fig. 4d). At V_{EG}/V_W< 1, the plates with different thicknesses have formed. It is obvious that in the presence of ethylene glycol, the phase-pure $[Bi_6O_6(OH)_3](NO_3)_3 \cdot 1.5H_2O$ cannot be obtained.

3.3 Photodegradation activity of single dye

Fig. 5a presents the photodegradation curves of RhB by the samples prepared at different pH values. After 30 min, 93.13% of RhB can be removed by the sample (BS1, pH=0.72), while 83.31%, 73.25%, 65.54% and 36.76% by the samples prepared at pH=0.95, 1.15, 5.38 and rutile TiO_2, respectively. Meanwhile, the self-degradation of RhB is 23.44%. We have measured the activity of Degussa P25 TiO_2. It is found that RhB can be degraded completely by Degussa P25 TiO_2 after 10-min UV irradiation. Its activity is higher than that of $[Bi_6O_6(OH)_3](NO_3)_3 \cdot 1.5H_2O$, since it is a mixture of anatase and rutile, high BET area and a high light absorbance, and so on.

View Article Online
DOI: 10.1039/C5RA14931B

Fig. 5c further gives their reaction kinetic curves. The apparent degradation kinetic rate (k_{BS1}=0.08481 min^{-1}) of RhB over BS1 is 1.53, 2.11, 2.60 and 6.90 times as high as those over the samples at pH=0.95, 1.15, 5.38 and rutile TiO_2, respectively. The photocatalytic degradation efficiencies of RhB over these samples follow the order: BS1> BS2 > BS3> BS5. It seems that the activities of the samples prepared at low pH values are higher than those at higher pH values. It should be pointed out that the BET areas of all the samples are lower than 2.0 $m^2 g^{-1}$. The similar results are also reported in the other reports. [11-13] Thus, the BET area has little influence on the activity in our study. As discussed above, the phase purity of the product is sensitive to the pH value. We hold that under an acidic preparation condition, H^+ ions could endow $[Bi_6O_6(OH)_3](NO_3)_3 \cdot 1.5H_2O$ with the positively charged surfaces. The surface charge properties would affect the surface adsorption nature of catalyst.

Generally, the surface oxygen vacancies are the active sites for molecular oxygen adsorption, thus the formation of oxygen vacancies on material surface is a prerequisite to molecular oxygen activation. Li et al. have reported that under common condition, less oxygen vacancies are present on the surface of TiO_2. [16] On the other hand, oxygen vacancy as one kind of point defect can promote the separation of photo-induced electrons and holes, leading to a high activity. Ye et al. [22] have reported that because of the low bond energy and long bond length of Bi–O, the unique atomic structure of bismuth facilitates the formation of oxygen vacancies under UV light irradiation. $[Bi_6O_6(OH)_3](NO_3)_3 \cdot 1.5H_2O$ consists of both $[Bi_2O_2]^{2+}$ and anions (OH^-, NO_3^-) layers, [15] thus oxygen vacancies could form through the breakage of Bi–O bond under UV irradiation. Herein, whether oxygen vacancies formed or not is still elusive. Limited by our research conditions, however, it is difficult for us to quantitatively investigate defects at present. Moreover, Cui *et al.* [23]

View Article Online
DOI: 10.1039/C5RA14931B

have reported that after phosphate modification, the increase of surface acidity favors for the O_2 adsorption on the TiO_2 surfaces, which enhances photogenerated charge separation. What is more, they have also demonstrated that after being modified by different sodium phosphates (Na_3PO_4, Na_2HPO_4, NaH_2PO_4, and H_3PO_4), the crystal phase and crystallinity of TiO_2 have not changed, although the phosphate groups have been anchored on the TiO_2 surfaces. They further reported that the surface modification of TiO_2 by H_3PO_4 or H_2SO_4 can chemically adsorb a large amount of O_2. [23] Therefore, we could infer that the surface acidity of $[Bi_6O_6(OH)_3](NO_3)_3 \cdot 1.5H_2O$ prepared at low pH values (with HNO_3) favors for the adsorption of O_2, leading to photogenerated charge separation. Summarily, the surface acidity of $[Bi_6O_6(OH)_3](NO_3)_3 \cdot 1.5H_2O$ is an important factor affecting the photocatalytic activity.

Typically, the light absorption properties of the samples prepared at different pH values were characterized by UV-vis diffuse reflection spectroscopy (UV-DRS) (Fig. 5e,f). The BS1 sample prepared at pH=0.72 has a higher absorbance than the others at pH=1.15, 0.95 and 0.83 in the UV region. The band gap of $[Bi_6O_6(OH)_3](NO_3)_3 \cdot 1.5H_2O$ can be calculated using Equation (3) as follows [24]:

$$\alpha h\nu = A\,(h\nu - E_g)^{n/2} \quad (3)$$

where α, $h\nu$, A, and E_g are optical absorption coefficient, photonic energy, proportionality constant and band gap, respectively. By extrapolating the straight line to the *x*-axis in Tauc plot (Fig. 5f), the band gaps are estimated to be 3.33 eV, 3.38 eV, 3.35 eV and 3.32 eV for the samples prepared at pH=0.83, 0.72, 0.95 and 1.15, respectively. For layered BiOCl, Zhang *et al.* have reported that the typical layered structure can provide a space large enough to polarize the related atoms and orbitals, resulting in the formation of dipoles. [25] The induced dipoles favor for the efficient

View Article Online
DOI: 10.1039/C5RA14931B

separation of hole–electron pair. From Tauc plot in Fig.5f we can know that $[Bi_6O_6(OH)_3](NO_3)_3 \cdot 1.5H_2O$ has an indirect-transition band-gap. For an indirect transition band gap, the excited electrons have to travel a certain space distance to reach conduction band. [25,26] Although an extra energy is needed, the recombination probability of photogenerated electrons and holes can be reduced greatly, leading to an improved photocatalytic activity. [25,26] To conclude, there is no obvious difference for their UV-DRS spectra.

Also, we have investigated the photoactivities of the samples prepared at different temperatures for the degradation of RhB (Fig. 5b,d). After reaction for 30 min, the removal efficiencies of RhB by the BS8, BS9, BS11 BS13 and BS14 samples are 37.18%, 87.95%, 93.13%, 90.01% and 67.79%, respectively. The apparent reaction rate constant of BS11 is 0.08481 min^{-1}, which is 6.3, 1.29, 1.17 and 2.47 times as high as that of BS8, BS9, BS13 and BS14, respectively. It is obvious that the BS11 sample obtained at 180 ^oC for 24 h shows the highest activity among them. Due to their similar BET areas (<2 m^2g^{-1}), its high activity can be attributed to the high crystallinity. A high crystallinity means that the samples possess less bulk defects, [18] which could reduce the recombining rate, leading to an improved activity.

3.4 Photocatalytic reaction mechanism and cycle stability

In previous study, [27,28] Honda et al. have demonstrated that the primary step of RhB degradation is N-deethylation, in which the electrons from the excited singlet RhB^* transport to CdS in the RhB/CdS system under visible light irradiation. Further, they have confirmed that RhB can undergo one-electron oxidation by investigating the cyclic voltammogram of RhB. Besides, Hu et al. [29] have reported that for a single electron transfer (SET) mechanism, the N-deethylation process is initiated by the

View Article Online
DOI: 10.1039/C5RA14931B

excitation of dye, followed by an electron transfer to catalyst. Subsequently, the resultant dye radicals hydrolyze to lose one alkyl group. Further, they have proved that N-deethylation of RhB arises from the hydrolysis of the cationic dye radical in the absence of active oxygen species. [29] In our study, there is no hypsochromic shift of the absorption maximum of RhB (Fig. 6a), but an obvious hypsochromic shift can be observed in the VO_2^+/RhB system. [29] Thus, in our study, the cleavage of whole conjugated chromophore structure of RhB, instead of the N-deethylation, may occur. The previous reports reported that the mineralization of dyes is mainly attributed to the formation of active oxygen species. [22,26-29] Thus oxygen species ($O_2^{-\cdot}$) could form in our experiments.

Herein, the trapping experiments are conducted to determine the active species, in which $Na_2C_2O_4$ and dimethyl sulphoxide (DMSO) are employed as the scavengers of hole and hydroxyl radical, respectively (Fig. 6b). When adding DMSO in reaction solution, 34.3% of RhB was degraded; while 38.5% of RhB was degraded when adding $Na_2C_2O_4$. We could deduce that over $[Bi_6O_6(OH)_3](NO_3)_3 \cdot 1.5H_2O$, RhB is oxidized simultaneously by both holes and hydroxyl radicals.

Thus, a degradation pathway of RhB is proposed, as shown in Fig. 6c. It is well-known that the organic radical species (RhB^*) resulted from the photosensization of RhB can facilely react with O_2 to produce peroxide free radicals, which can further initiate a series of radical chain reactions and finally mineralize organic compounds. At the same time, the conduction band (-0.9 V *vs*. N.H.E.) of $[Bi_6O_6(OH)_3](NO_3)_3 \cdot 1.5H_2O$ is more negative than the reduction potential ($E^\circ(O_2/O_2^{-\cdot})$ = -0.33 V *vs*. N.H.E.) of O_2, indicating that oxygen species ($O_2^{-\cdot}$) could be generated during the degradation process; whereas its less positive valence band (+2.48 V *vs*. N.H.E.) indicates that H_2O cannot be oxidized to form ·OH ($E^\circ(\cdot OH/H_2O)$ = +2.68 V

View Article Online
DOI: 10.1039/C5RA14931B

vs. N.H.E.). [12,30] As reported in the literature, [31] $O_2^{-\cdot}$ is unstable in aqueous solution and is easily decomposed into ·OH. In our experiment, both h^+ and ·OH are main active species, but the generation of $O_2^{-\cdot}$ could be the prerequisite step to the generation of ·OH.

To investigate the stability of $[Bi_6O_6(OH)_3](NO_3)_3 \cdot 1.5H_2O$ under UV light irradiation, the degradation reaction of RhB dye over the BS1 sample was cycled for three times (Fig. 6d). It is noteworthy that after three cycles, its degradation efficiency is only reduced by 4.2%, indicating a good stability of $[Bi_6O_6(OH)_3](NO_3)_3 \cdot 1.5H_2O$.

3.5 Photodegradation of MB/MO and RhB/MO mixture dye wastewater

Generally, more than one dye is contained in practical wastewater. In order to simulate practical wastewater, the degradations of MB/MO and RhB/MO mixture dyes were investigated over the BS1 sample. As shown in Fig. 6a and 7a-d, the maximum absorption peaks positions of MB, MO and RhB do not change in single dye or mixture dye solution, suggesting that no intermediates are produced. After 30 min UV irradiation, the removal ratios of MB(Single dye), MO(Single dye), MB(MB/MO), MO(MB/MO) are 56%, 27.68%, 73.87%, 47.86%, respectively. Especially, the removal ratio of MB(MB/MO) reaches 71% after 10 min UV irradiation. It is surprising that the removal efficiencies of MB and MO in the MB/MO mixture solution are greatly higher than those in single dye, respectively. It is obvious that a mutual promoting effect may occur between MO and MB. In Fig.s 7e and 7g, the adsorption value of MB is 55.88% in MB/MO mixture solution, which is 3.9 times as high as that (14.5%) in single MB solution. Herein, adsorption is mainly a physical process, in which dye molecules adsorb on the catalyst surface to reach an adsorption-desorption balance before light on. Generally, the adsorption of dye

View Article Online
DOI: 10.1039/C5RA14931B

molecules on the catalyst surface is the prerequisite for a degradation reaction. At the same time, the adsorption value of MO is 14.23% in MB/MO mixture solution, which is 13.3 times higher than that in single MO solution. We hold that the negatively-charged MO (or positively-charged MB) may have improved the adsorption of positively-charged MB (or negatively-charged MO) on the $[Bi_6O_6(OH)_3](NO_3)_3 \cdot 1.5H_2O$ surface. Thus, there is a strong interaction between the components in the MB/MO mixture solution.

However, such a mutual promoting effect is not obvious in RhB/MO mixture solution. Compared with single dye solution, however, the adsorption abilities of both RhB and MO in RhB/MO solution have not changed obviously, but the degradation activity of RhB decreases obviously. Fig. 7h clearly shows that their photocatalytic removal ratios decrease in the order as follows: MB(MB/MO) > RhB > MB > MO(MB/MO) > RhB(RhB/MO) > MO(RhB/MO) ≈ MO. After 60-min irradiation, the removal ratios of MB(MB/MO), MO(MB/MO), RhB(RhB/MO) and MO(RhB/MO) mixture dye solution are 76.30% , 63.78%, 73.02% and 46.75%, respectively. It is easily understood that in the RhB/MO mixture solution, the reduced activity results primarily from the competitive adsorption on the catalyst surface.

Our experiment results show that in MB/MO solution, the mutual promotion effect of both MB and MO on adsorption and degradation could mainly be resultant from the electrostatic interaction between cationic MB and anionic MO. Our Zeta potential measurements show that the surface of $[Bi_6O_6(OH)_3](NO_3)_3 \cdot 1.5H_2O$ is positively charged. Thus, the anionic dye molecules adsorb on catalyst and are activated by catalyst preferentially, as shown in Fig. 8. It should point out that the adsorption of MB in single MB dye solution may be due to the two donor atoms (S, N) with lone pair electrons. As shown in Fig. 8, we assume that in MB/MO solution, the

View Article Online
DOI: 10.1039/C5RA14931B

adsorption of MB can be improved greatly through the electrostatic interaction with MO preferentially adsorbed on catalyst. In turn, the adsorbed MB on the catalyst can also promote the further adsorption of MO on the catalyst. Compared RhB-MO with single dye, on the other hand, the adsorption ability of RhB or MO has not change nearly (Fig. 7f). However, the degradation ratio of RhB is reduced, while that of MO does not change obviously (Fig. 7h). We could deduce that the electrostatic interaction between MO and RhB may be weaker than that between MO and MB. This could be because MB and RhB have different molecular structures (Fig. 8). It has been reported that the degradation efficiency of MO is high under acidic condition. [30] As an anionic dye, MO contains azo group (-N=N-) that links to aromatic sp2-hybridized C-atoms (Fig. 8). As a cationic dye, RhB contains a carboxyl group that can hydrolyze to release H^+. The adsorption of H^+ favors to increase the positive charge of catalyst, thus slightly promoting the adsorption of MO. At the same time, the hydrolyzed RhB is endowed with a negative charge due to the presence of COO^-, thus a competitive adsorption could occur between them. As a result, the degradation ratio of RhB decreased. To conclude, it is the molecule structure and the charging properties of dye that lead to a different removal efficiency. It should be pointed out that the true mechanism for mixture dye solution needs further study in future.

4. Conclusions

The pH value of precursor solution has a significantly influence on the formation of $[Bi_6O_6(OH)_3](NO_3)_3 \cdot 1.5H_2O$. In the MB/MO mixture solution, the adsorption and the degradation of MB have been greatly improved by MO, which has been mainly attributed to their electrostatic interaction; while the degradation of RhB has been refrained obviously by MO due to the competitive adsorption between RhB and MO.

View Article Online
DOI: 10.1039/C5RA14931B

The different results for cationic MB and RhB are mainly ascribed to their different molecule structures. The finding is useful to promote the application of photocatalysis in cleaning practical wastewater.

Acknowledgments

This work is financially supported by National Science Foundation of China (21377060), the Project Funded by the Science and Technology Infrastructure Program of Jiangsu (BM201380277), Jiangsu Science Foundation of China (BK2012862), Six Talent Climax Foundation of Jiangsu (20100292), Jiangsu Province of Academic Scientific Research Industrialization Projects (JHB2012-10, JH10-17), the Key Project of Environmental Protection Program of Jiangsu (2013016, 2012005), A Project Funded by the Priority Academic Program Development of Jiangsu Higher Education Institutions (PAPD) sponsored by SRF for ROCS, SEM (2013S002) and “333” Outstanding Youth Scientist Foundation of Jiangsu (2011015).

View Article Online
DOI: 10.1039/C5RA14931B

References

1. A. Fujishima, Nature 1972, **238**, 37-38.
2. H. Suzuki, N. Komatsu, T. Ogawa, T. Murafuji, T. Ikegami and Y. Matano, Organobismuth chemistry, Elsevier, 2001.
3. S. Shimada, O. Yamazaki, T. Tanaka, M.L. Rao, Y. Suzuki and M. Tanaka, Angew. Chem. Int. Ed. 2003, **115**, 1889-1892.
4. P.K. Koech and M.J. Krische, J. Am. Chem. Soc. 2004, **126**, 5350-5351.
5. H. Qin, N. Yamagiwa, S. Matsunaga and M. Shibasaki, J. Am. Chem. Soc. 2006, **128**, 1611-1614.
6. A. Gagnon, M. St-Onge, K. Little, M. Duplessis and F. Barabé, J. Am. Chem. Soc. 2007, **129**, 44-45.
7. S.-F. Yin, M. Bao and S. Shimada, The 32nd Symposium on Heteroatom Chemistry (Ed. Michael THL), Tsukuba: Asahi Publishing Company 2005, 228-229.
8. N.M. Leonard, M.C. Oswald, D.A. Freiberg, B.A. Nattier, R.C. Smith and R.S. Mohan, J. Org. Chem. 2002, **67**, 5202-5207.
9. N. Srivastava, S.K. Dasgupta and B.K. Banik, Tetrahedron Lett. 2003, **44**, 1191-1193.
10. A.N. Christensen, M.-A. Chevallier, J. Skibsted and B.B. Iversen, J. Chem. Soc. Dalton, 2000, **1**, 265-270.
11. L. Xie, J. Wang, Y. Hu, Z. Zheng, S. Weng, P. Liu, X. Shi and D. Wang, Mater. Chem. Phys. 2012, **136**, 309-312.
12. L. Xie, J. Wang, Y. Hu, S. Zhu, Z. Zheng, S. Weng and P. Liu, RSC Adv. 2012, **2**, 9881-9886.

View Article Online
DOI: 10.1039/C5RA14931B

13. Y. Yang, H. Liang, N. Zhu, Y. Zhao, C. Guo and L. Liu, Chemosphere 2013, **93**, 701-707.
14. Y. Li, J. Liu and X. Huang, Nanoscale Res. Lett. 2008, **3**, 365-371.
15. N. Henry, M. Evain, P. Deniard, S. Jobic, F. Abraham and O. Mentré, Z. Naturforsch. B 2005, **60**, 322-327.
16. J. Li, Y. Yu and L. Zhang, Nanoscale 2014, **6**, 8473-8488.
17. L. Xiao, Y. Zhao, J. Yin and L. Zhang, Chem.-Eur. J. 2009, **15**, 9442-9450.
18. B. Ohtani, J. Photoch. Photobio. C, 2010, **11**, 157-178.
19. D.H. Kim, S.H. Kim, K. Lavery and T.P. Russell, Nano lett. 2004, **4**, 1841-1844.
20. J. Zhao, Q. Han, J. Zhu, X. Wu and X. Wang, Nanoscale, 2014, **6**, 10062-10070.
21. M. Lélias, P. Kooyman, L. Mariey, L. Oliviero, A. Travert, J. Van Gestel, J. Van Veen and F. Maugé, J. Catal. 2009, 267, 14-23.
22. L. Ye, L. Zan, L. Tian, T. Peng and J. Zhang, Chem. Commun. 2011, **47**, 6951-6953.
23. H. Cui, Y. Cao, L. Jing, Y. Luan and N. Li, ChemPlusChem, 2014, **79**, 318-324.
24. Y. Ohko, K. Hashimoto and A. Fujishima, J. Phys. Chem. A. 1997, **101**, 8057-8062.
25. K.-L. Zhang, C.-M. Liu, F.-Q. Huang, C. Zheng and W.-D. Wang, Appl. Catal. B-Environ. 2006, **68**, 125-129.
26. L. Ye, K. Deng, F. Xu, L. Tian, T. Peng and L. Zan, Phys. Chem. Chem. Phys. 2012, **14**, 82-85.
27. T. Watanabe, T. Takizawa and K. Honda, J. Phys. Chem. C 1977, **81**, 1845-1851.
28. T. Takizawa, T. Watanabe and K. Honda, J. Phys. Chem. C 1978, **82**, 1391-1396.
29. X. Hu, T. Mohamood, W. Ma, C. Chen and J. Zhao, J. Phys. Chem. B 2006, **110**, 26012-26018.

View Article Online
DOI: 10.1039/C5RA14931B

30. K. Wang, J. Xu, X. Hua, N. Li, M. Chen, F. Teng, Y. Zhu and W. Yao, J. Mol. Catal. A-Chem. 2014, **393**, 302-308.

31. M. Yin, Z. Li, J. Kou and Z. Zou, Environ. Sci. Technol. 2009, **43**, 8361-8366.

View Article Online
DOI: 10.1039/C5RA14931B

Title list of Tables and Figures

View Article Online
DOI: 10.1039/C5RA14931B

Fig. 6. UV-vis absorption spectra of rhodamine B (RhB) (a), degradation curves of RhB by the BS1 sample while adding dimethyl sulphoxide (DMSO) and $Na_2C_2O_4$ (b), degradation pathways of RhB (c) and the cycle experiment (d)

Fig. 7. UV-vis absorption spectra of (a) methylene blue (MB), (b) methyl orange (MO), MB-MO(c) and RhB-MO(d) solutions at different reaction times; Photodegradation curves (e, f) of different dyes solutions in 30 min; Adsorption (g) and removal ratio (h) histograms of different dye solutions in 30 min

Fig. 8. Schematic diagram of mutual interaction of MO with MB and RhB

View Article Online
DOI: 10.1039/C5RA14931B

Table 1

Table 1 Effect of pH value on the samples

Sample	Bismuth(III) (mmol)	Reagent	pH	Temperature (^{o}C)	Reaction time (h)
BS1	1	HNO_3	0.72	180	24
BS2	1	HNO_3	0.95	180	24
BS3	1	/	1.15	180	24
BS4	1	HNO_3+$NH_3 \cdot H_2O$	3.51	180	24
BS5	1	HNO_3+$NH_3 \cdot H_2O$	5.38	180	24
BS6	1	HNO_3+$NH_3 \cdot H_2O$	7.36	180	24
BS7	1	HNO_3+$NH_3 \cdot H_2O$	9.05	180	24

View Article Online
DOI: 10.1039/C5RA14931B

Table 2

Table 2 Effects of temperature, reaction time and Bi(III) concentration on the samples

Sample	Bismuth(III) (mmol)	Temperature (^{o}C)	Reaction time (h)
BS8	1	90	24
BS9	1	120	24
BS10	1	150	24
BS11	1	180	24
BS12	1	180	30
BS13	1	180	18
BS14	1	180	12
BS15	0.5	180	24
BS16	1.5	180	24
BS17	2.0	180	24

View Article Online
DOI: 10.1039/C5RA14931B

Table 3

Table 3 Effect of volumetric ratio of ethylene glycol (EG) to water (W) on the samples

Sample	Bismuth(III) (mmol)	Solvent (V_{EG}/V_W)	Temperature (^oC)	Reaction time (h)
BS21	1.0	1/0	180	24
BS22	1.0	3/1	180	24
BS23	1.0	2/1	180	24
BS24	1.0	1.5/1	180	24
BS25	1.0	1/1	180	24
BS26	1.0	0.67/1	180	24
BS27	1.0	0.5/1	180	24
BS28	1.0	0.33/1	180	24
BS29	1.0	0/1	180	24

View Article Online
DOI: 10.1039/C5RA14931B

Table 4

Adsorption and degradation ratios for single methylene blue (MB), single methylene orange (MO), single rhodamine B (RhB), MB/MO, RhB/MO solutions

Dyes	Adsorption (at 30 min)	Degradation (at 30 min)	Degradation (at 60 min)
MB	14.34%	56.00%	/
MO	1.07%	27.68%	/
RhB	2.62%	57.46%	/
MB(MB/MO)	55.88%	73.87%	76.30%
MO(MB/MO)	14.23%	47.86%	63.78%
RhB(RhB/MO)	2.51%	42.78%	73.02%
MO(RhB/MO)	1.25%	28.51%	46.75%

View Article Online
DOI: 10.1039/C5RA14931B

Fig. 1

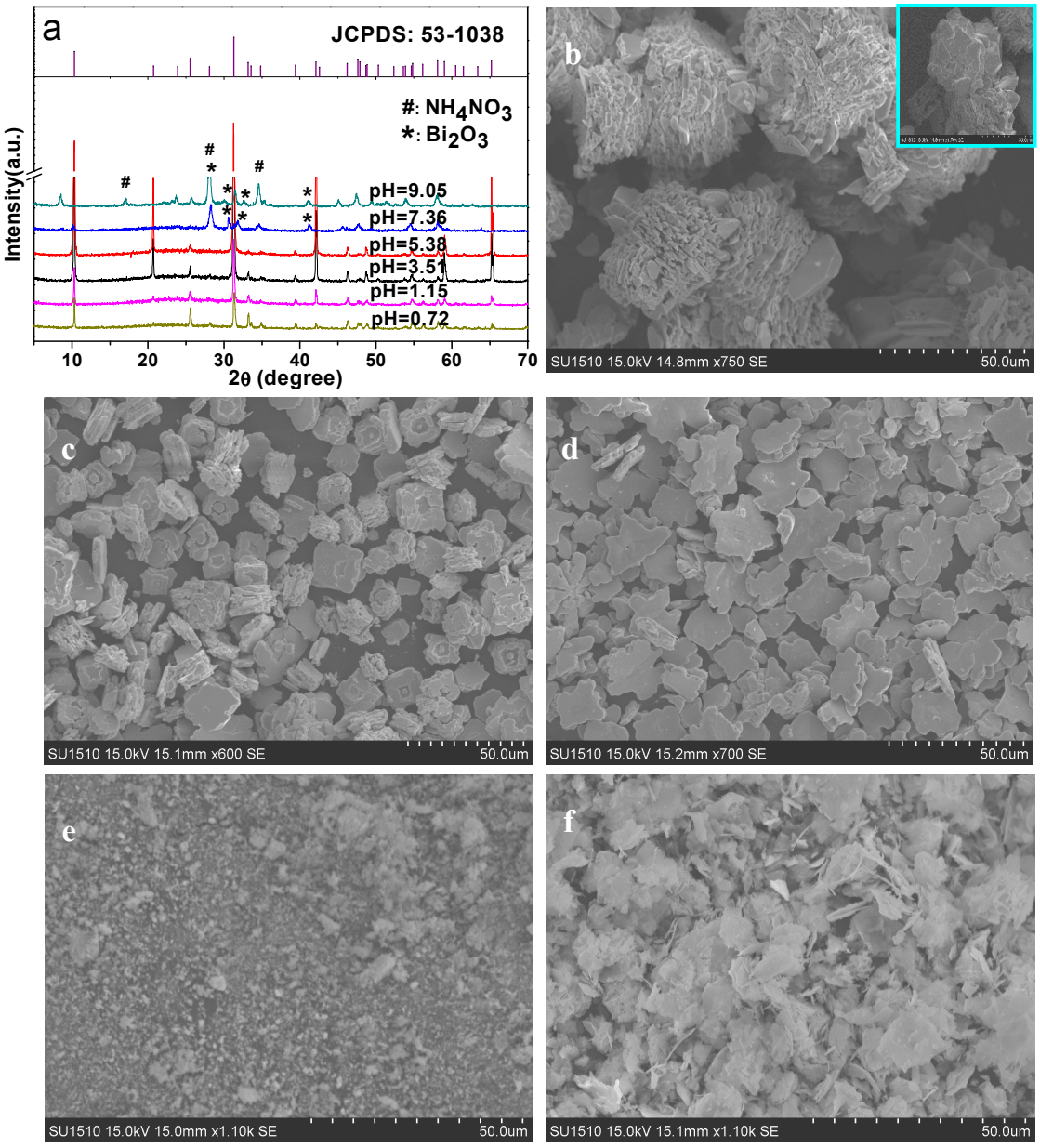

View Article Online
DOI: 10.1039/C5RA14931B

Fig. 2

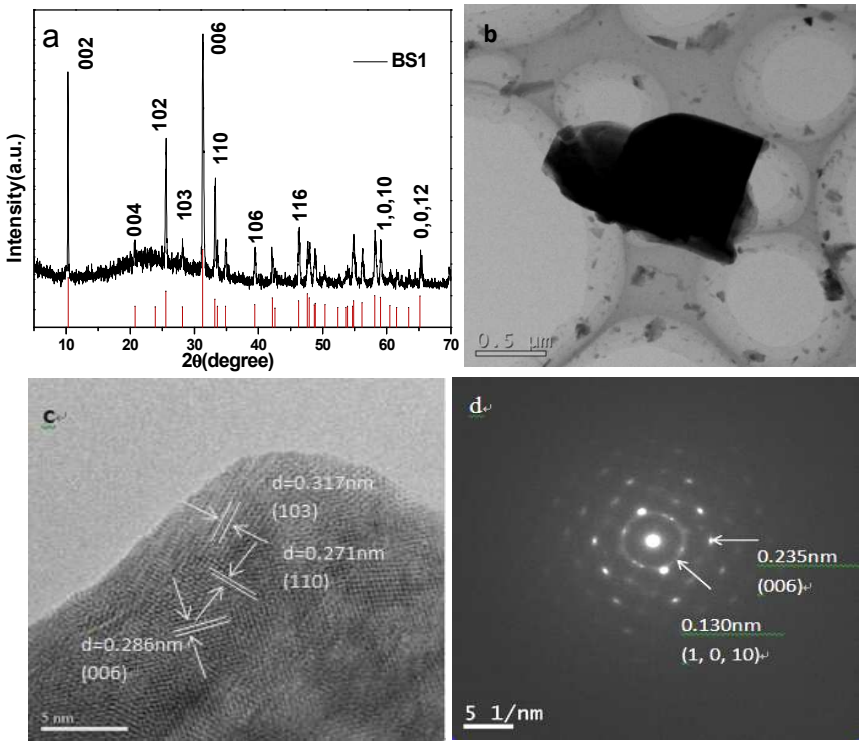

View Article Online
DOI: 10.1039/C5RA14931B

Fig. 3

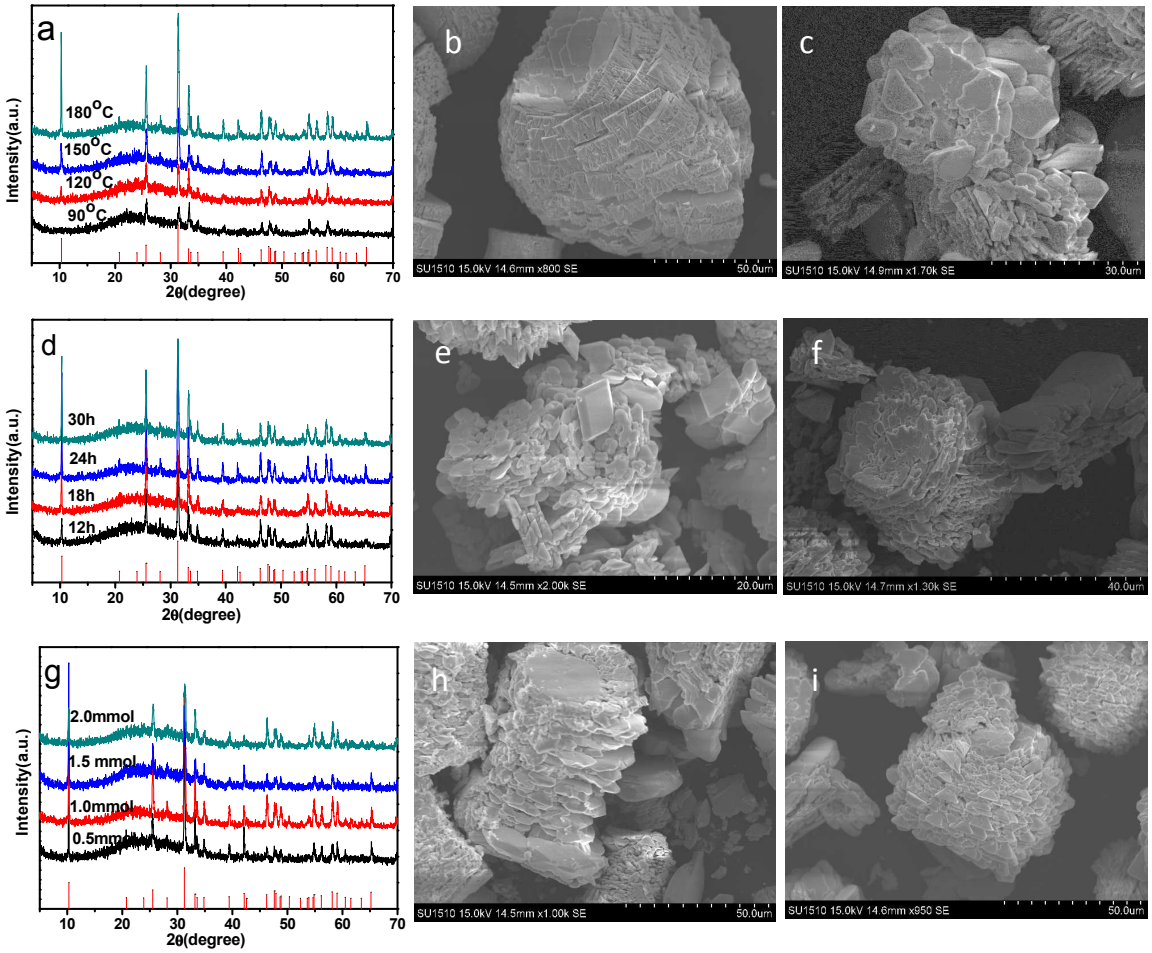

View Article Online
DOI: 10.1039/C5RA14931B

Fig. 4

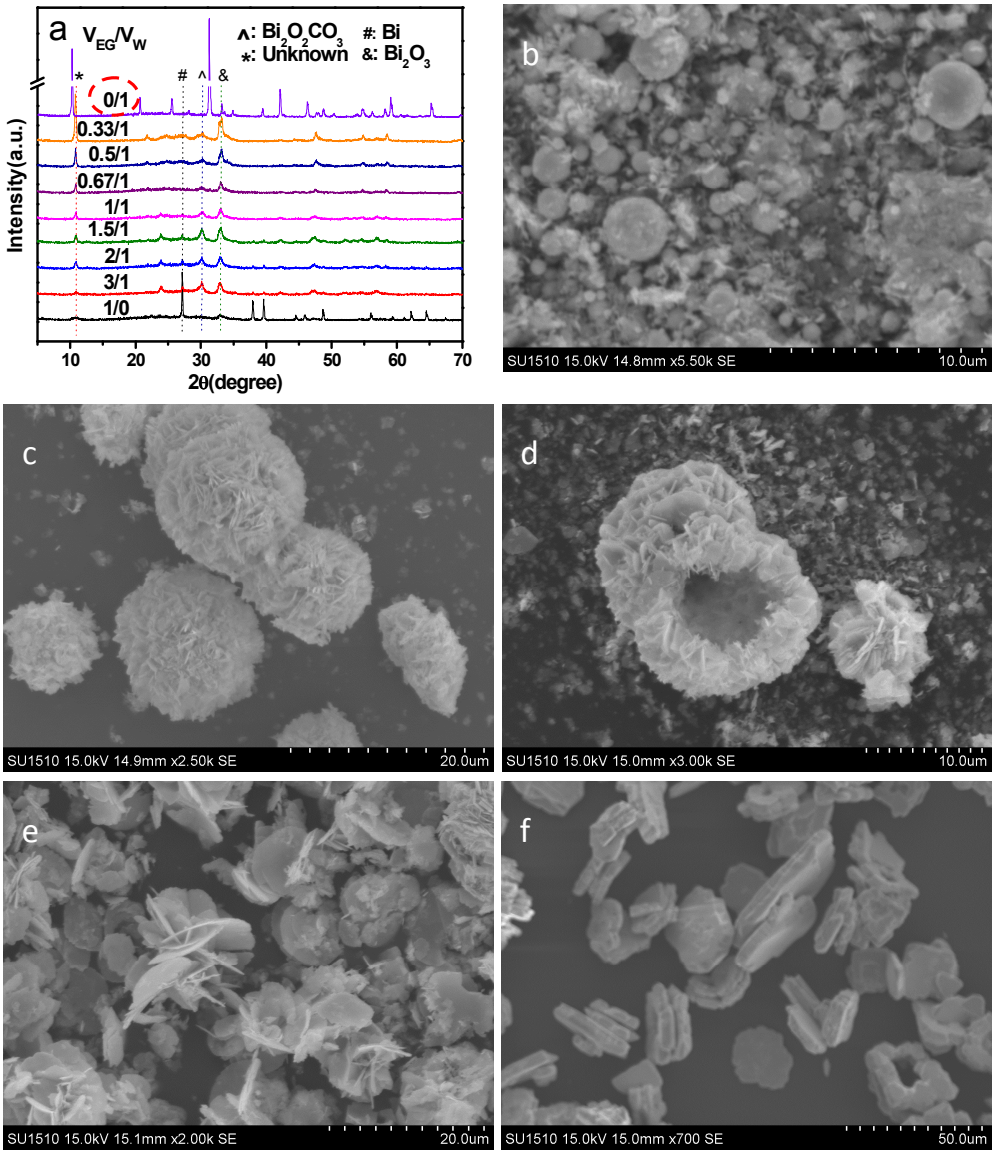

View Article Online
DOI: 10.1039/C5RA14931B

Fig. 5

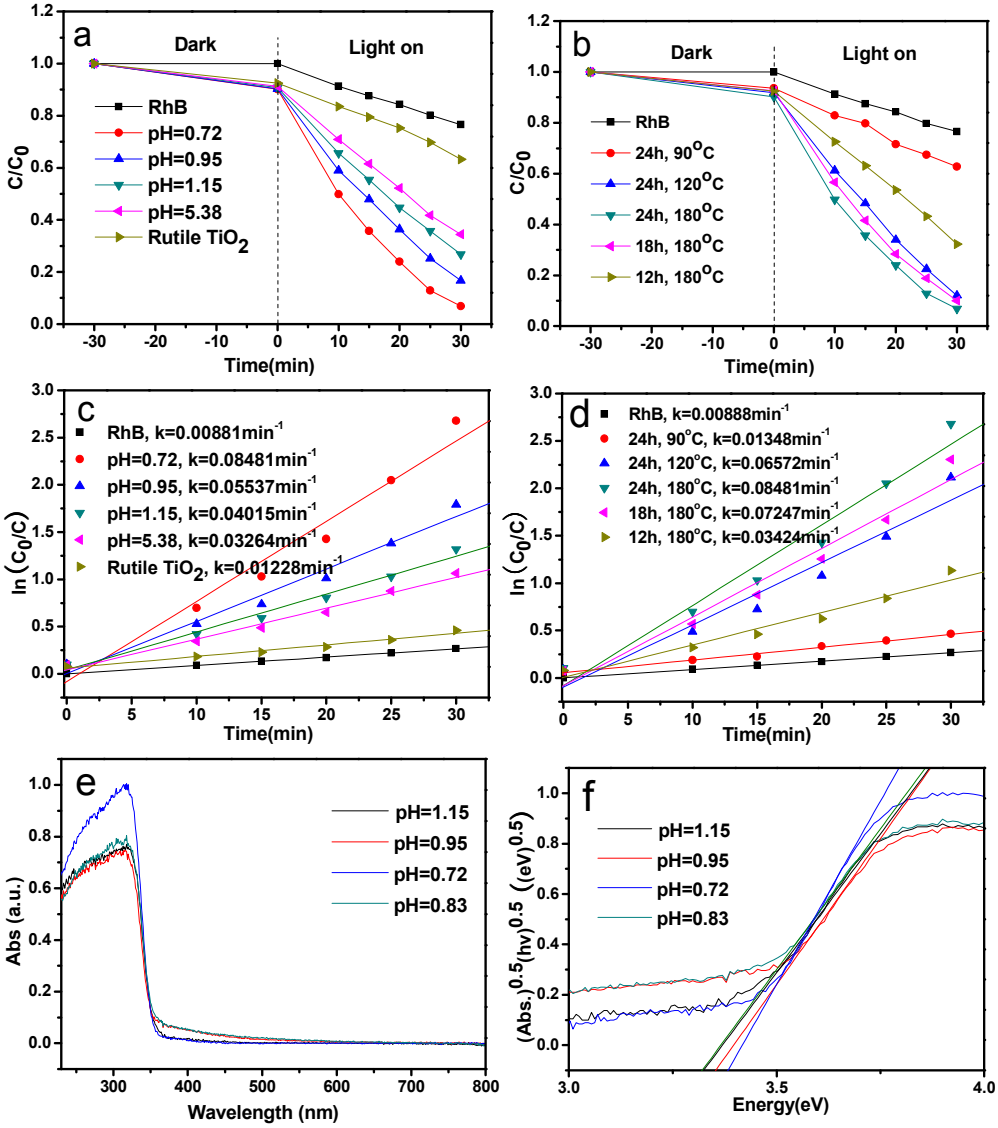

View Article Online
DOI: 10.1039/C5RA14931B

Fig. 6

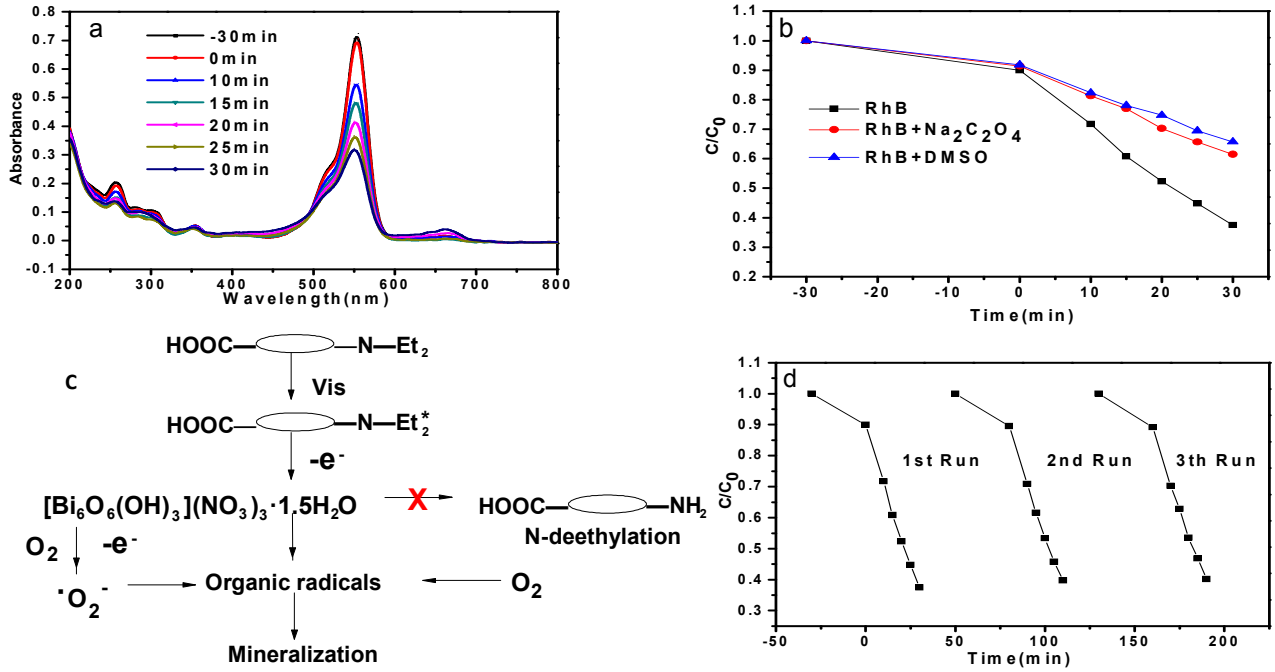

View Article Online
DOI: 10.1039/C5RA14931B

Fig. 7

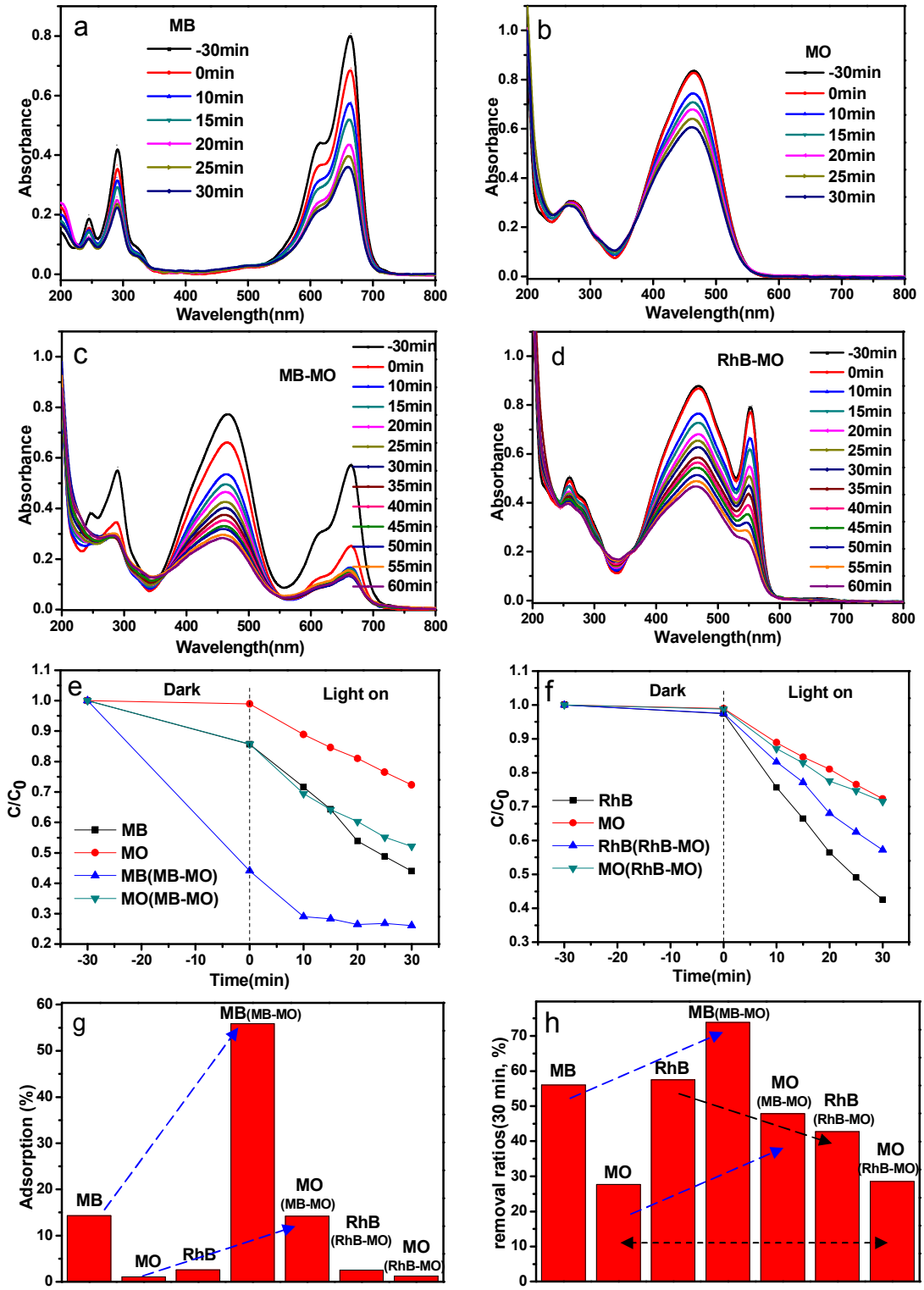

View Article Online
DOI: 10.1039/C5RA14931B

Fig. 8

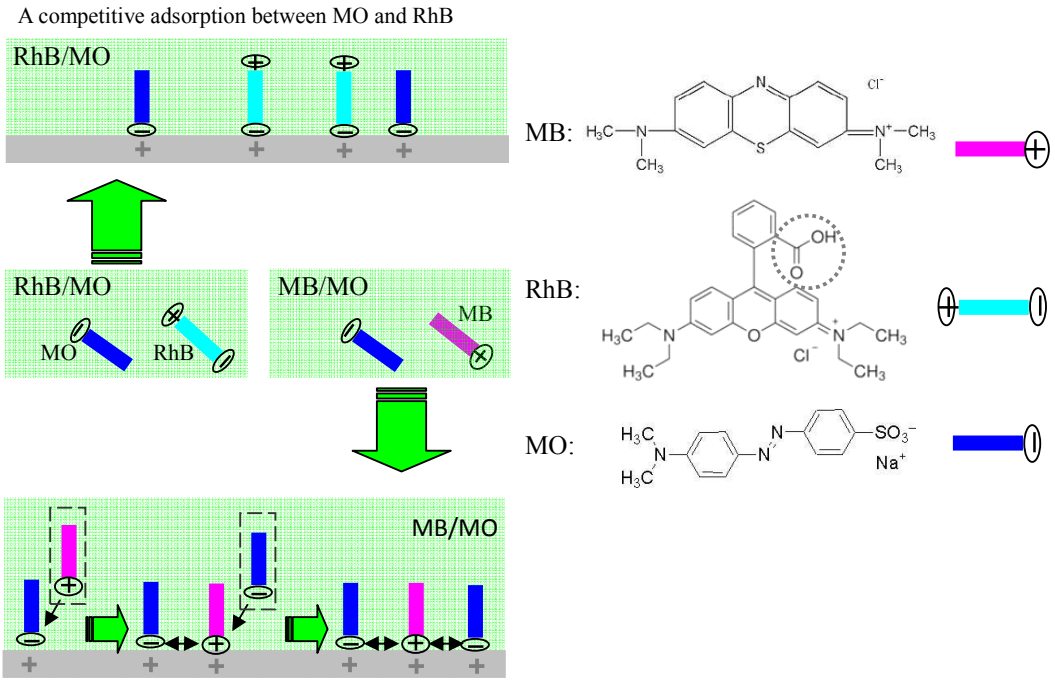

Promoted adsorption between MB and MO via an electrostatic force

View Article Online
DOI: 10.1039/C5RA14931B

Table of Contents Entry (TOC)

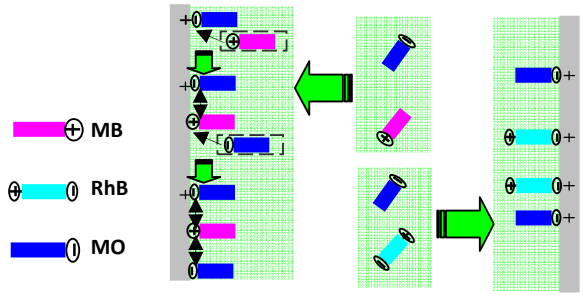

Diagram of interaction of MO with MB (RhB) in mixture solution